# Modified Mean-Power-Distribution-Based Nonlinear Coefficient Optimization for Digital Back-Propagation in High-Baud-Rate Optical Systems

Meng Yang, Pinjing He, Aiying Yang, and Peng Guo

***Abstract*—The digital back-propagation (DBP) is an effective algorithm to compensate for the nonlinear impairments in high-baud-rate and long-haul optical systems. The nonlinear coefficient of the DBP algorithm is optimized based on the mean power at the step position. However, when the number of steps per span of the DBP algorithm is fixed below the optimum step number to constrain computational complexity, the optimum nonlinear coefficient is sensitive to the number of steps per span. In this paper, we used the average value of the mean power over the step size to optimize the nonlinear coefficient of the DBP algorithm. The modified mean-power-distribution-based nonlinear coefficient optimization scheme was applied to constant step-size DBP (MMPD-CS-DBP) and logarithmic step-size DBP (MMPD-LS-DBP) algorithms in 30 × 80 km SSMF single-channel Nyquist 64 GBaud and 5 × 64 GBaud Nyquist WDM polarization multiplexing 16QAM systems, respectively. Simulation results showed that the optimum nonlinear coefficient of the MMPD-CS-DBP and MMPD-LS-DBP algorithms was the nonlinear coefficient of the optical fiber and was robust to the number of steps per span.**

***Index Terms*—High-baud-rate optical systems, digital back-propagation, nonlinear coefficient optimization.**

## I. Introduction

OVER the last two decades, the growth of capacity demands has led to the increase in data rate per wavelength division multiplexing (WDM) channel [1], [2], [3]. Significant research has been made to increase the single-channel data rate by pushing both the baud rate and modulation format order [4], [5], [6]. Optical transmission of the per-channel data rate of 400 Gb/s has emerged as a natural and promising step as the next-generation transport standard [7], [8], [9].

However, in high-baud-rate and long-haul optical transmission systems, signal propagation in nonlinear optical fiber significantly suffers from transmission impairments, which include chromatic dispersion (CD), Kerr nonlinearity of self-phase modulation (SPM), cross-phase modulation (XPM), and four-wave mixing (FWM) [10], [11], [12], [13]. The nonlinear Schrödinger equation (NLSE) describes the interactions among CD, SPM, and inline optical amplifier noise. In recent years, the digital back-propagation (DBP) algorithm has received much attention due to its effective performance of nonlinearity compensation (NLC), which inverts the distortions of CD and SPM using the split-step Fourier method (SSFM) [14], [15], [16]. For the constant step-size DBP (CS-DBP) algorithm, the nonlinear coefficient is optimized based on the mean power distribution over one span of single-mode fiber (SSMF) [14]. However, the CS-DBP algorithm requires many steps, causing high computational complexity, especially in high-baud-rate and long-haul transmissions. One way to reduce the computational complexity of the CS-DBP algorithm is to modify the step size distribution [17], [18]. R. Asif et al. proposed a logarithmic step-size DBP (LS-DBP) algorithm [17]. J. Zhang et al. introduced an attenuation adjustment factor to optimize the logarithmic step size. The LS-DBP can reduce the optimum step number (the minimum step number per span to achieve the maximum Q-factor) of the CS-DBP algorithm [18]. Another way is to improve the nonlinear coefficient optimization scheme [19], [20], [21], [22]. D. Rafique et al. optimized the nonlinear coefficient based on the correlation of signal power in neighboring symbols [19]. M. Secondini et al. proposed an enhanced DBP algorithm that combined the benefits of split-step and perturbation-based approaches to reduce computational complexity [20] and more recently, a smoothing learned DBP using a neural network was proposed to reduce the computational complexity of DBP algorithm [21]. In our previous work, a nonlinear coefficient optimization scheme based on the peak power distribution of Gaussian pulse was proposed to improve the NLC performance of the CS-DBP algorithm for a 2400 km SSMF 32 GBaud polarization-multiplexing (PM) 16 quadrature amplitude modulation (16QAM) optical transmission system [22].

In recent years, attention has been paid to the nonlinearity compensation effectiveness of the DBP algorithm for single-channel optical transmission systems with baud rate up to 200 Gbaud [23], [24]. H. N. Tan et al. studied the effectiveness of nonlinearity compensation techniques and found that the

Manuscript received 8 August 2022; revised 9 October 2022; accepted 21 October 2022. Date of publication 26 October 2022; date of current version 7 November 2022. This work was supported in part by the National Natural Science Foundation of China under Grant 61427813 and in part by the Open Fund of IPOC (BUPT) under Grant IPOC2018B003. *(Corresponding author: Aiying Yang.)*

The authors are with the Key Laboratory of Photonics Information Technology, Ministry of Industry and Information Technology, School of Optics and Photonics, Beijing Institute of Technology, Beijing 100081, China (e-mail: 3120205323@bit.edu.cn; hepinjing93@gmail.com; yangaiying@bit.edu.cn; guopeng0304@bit.edu.cn).

Digital Object Identifier 10.1109/JPHOT.2022.3217341

benefit of the DBP algorithm with 10 steps/span was decreased by more than 3 dB when the baud rate was increased to 64 Gbuad in a 2400 km SSMF PM-16QAM system [23]. N. V. Dien et al. proposed an advanced LS-DBP algorithm for optical transmission systems with a baud rate up to 200 Gbaud, in which the logarithmic step-size needed to be optimized [24]. C. Häger et al. proposed a sub-band division solution to reduce the required linear filter size [25].

Both in the CS-DBP and LS-DBP algorithms, when the number of steps per span is fixed below the optimum step number to constrain computational complexity, the optimum nonlinear coefficient is smaller than that of the optical fiber. And the optimum nonlinear coefficient is sensitive to the number of steps per span [13]. Therefore, it is necessary to optimize the nonlinear coefficient of the DBP algorithm. In this paper, a modified mean-power-distribution-based nonlinear coefficient optimization scheme is proposed. Firstly, we have analyzed the peak power distribution of the root-raised-cosine (RRC) pulses over 30 × 80 km SSMF using the SSFM in single-channel Nyquist 64 GBaud optical transmission system. Simulation results show that the peak power distribution of the RRC pulses will converge to the mean power distribution after one span of SSMF transmission. Then, we use the average value of the mean power over the step size to optimize the nonlinear coefficient of DBP algorithm. Finally, the modified mean-power-distribution-based nonlinear coefficient optimization scheme is applied with CS-DBP (MMPD-CS-DBP) and LS-DBP (MMPD-LS-DBP) algorithms, respectively. We investigate the optimum nonlinear coefficient and the nonlinearity compensation performance of the MMPD-CS-DBP and MMPD-LS-DBP algorithms in the simulation transmissions of single-channel Nyquist 64 GBaud and 5 × 64 GBaud Nyquist WDM PM-16QAM symbols over 30 × 80 km SSMF, respectively. Simulation results show that the optimum nonlinear coefficient of the MMPD-CS-DBP and MMPD-LS-DBP algorithms is that of the optical fiber and is robust to the number of steps per span.

## II. Theory and Algorithm

### A. Digital Back-Propagation Algorithm

Ignoring amplified spontaneous emission (ASE) noise, the signal propagation (dual polarization) in optical fiber can be described by the NLSE [15].

$$\frac{\partial U_{i(i=x,y)}(T,z)}{\partial z} = \left( \underbrace{j\frac{8}{9}\gamma e^{-\alpha z} P_0(z) |U_x(T,z) + U_y(T,z)|^2}_{\boldsymbol{N}(U)} - \underbrace{j\frac{\beta_2}{2}\frac{\partial^2}{\partial T^2}}_{\boldsymbol{D}(U)} \right) U_{i(i=x,y)}(T,z) \tag{1}$$

where $U_{i(i=x,y)}(T,z)$ represents the normalized amplitude of $x$ and $y$ polarization at time $T$ and distance $z$. The fiber parameters $\alpha$, $\beta_2$, and $\gamma$ are the attenuation, group velocity dispersion, and nonlinear coefficients. $P_0(z)$ is the peak power of $U_{i(i=x,y)}(T,z)$ at distance $z$. $\boldsymbol{N}(U)$ and $\boldsymbol{D}(U)$ are the nonlinear and linear operators, respectively.

In the NLC steps of the DBP algorithm, nonlinear-phase de-rotation operator $\boldsymbol{N}^{-1}(U)$ is expressed as

$$\begin{aligned} \boldsymbol{N}^{-1}(U) &= e^{-j\psi_{x\mathrm{NL}}} = e^{-j\psi_{y\mathrm{NL}}} \\ &= e^{-j\frac{8}{9}\gamma_{\mathrm{DBP,n}} L_{\mathrm{eff}} \left( \left| U_{x,\boldsymbol{D}^{-1}(U)} \right|^2 + \left| U_{y,\boldsymbol{D}^{-1}(U)} \right|^2 \right)} \end{aligned} \tag{2}$$

where $\psi_{x\mathrm{NL}}$ and $\psi_{y\mathrm{NL}}$ are the nonlinear phase of $x$ and $y$ polarization, respectively. $U_{x,\boldsymbol{D}^{-1}(U)}$ and $U_{y,\boldsymbol{D}^{-1}(U)}$ are the signals with linear CD compensation of $x$ and $y$ polarization, respectively. $\gamma_{\mathrm{DBP,n}}$ is the $n$th nonlinear coefficient of the DBP algorithm and needs to be optimized. $L_{\mathrm{eff}}$ is the effective fiber length expressed as $\left(1 - e^{-\alpha \Delta z_n}\right)/\alpha$. $\Delta z_n$ is the $n$th step size of the DBP algorithm. In the CS-DBP algorithm, $\Delta z_n$ is calculated by [14]

$$\Delta z_n = \frac{L}{N}, n = 1, 2, \ldots, N \tag{3}$$

where $L$ is the span length of optical fiber. $N$ is the step number per span. In the LS-DBP algorithm, $\Delta z_{\mathrm{n}}$ is calculated by [17]

$$\Delta z_n = -\frac{1}{\alpha} \ln \left( \frac{1 - n\delta}{1 - (n-1)\delta} \right), n = 1, 2, \ldots, N \tag{4}$$

where $\delta$ is expressed as $\delta = \left(1 - e^{-\alpha L}\right)/N$.

### B. The Modified Mean-Power-Distribution-Based Nonlinear Coefficient Optimization Scheme

(1) and (2) show that the value of $\gamma_{\mathrm{DBP,n}}$ is related to the peak power $P_0(z)$. In Nyquist optical transmission systems, RRC pulse shaping is usually applied at the transmitter, together with the matched RRC filter at the receiver, to reduce the inter-symbol interference (ISI) [26]. The modulated RRC pulses are expressed as

$$s(t) = \sum_{n=-\infty}^{\infty} b_n g\left(t - nT_s\right) \tag{5}$$

where $b_n$ is the $n$th modulation symbol. $g(t)$ is the single RRC pulse and is expressed as

$$g(t) = \frac{4a\cos((1+a)\pi t/T_{\mathrm{s}}) + T_{\mathrm{s}}^2 \sin((1-a)\pi t/T_{\mathrm{s}})/t}{\pi\sqrt{T_{\mathrm{s}}}(1 - (4at/T_{\mathrm{s}})^2)} \tag{6}$$

where $a$ is the roll-off factor. $T_{\mathrm{s}} = \frac{1}{R_{\mathrm{B}}}$ is the symbol period, and $R_{\mathrm{B}}$ is the baud rate of system.

We have analyzed the peak power evolution of the RRC pulses $s(t)$ using the SSFM over 30 × 80 km SSMF with $\alpha = 0.2$ dB/km, $\beta_2 \approx -21$ ps$^2$/km, and $\gamma = 1.2$ W$^{-1}$km$^{-1}$ in single-channel Nyquist 64 GBaud system. The step size of SSFM is 1 km. The center frequency is 193.1 THz. At the end of span, an EDFA with 16 dB gain is used to compensate for the fiber attenuation. Fig. 1 shows the normalized peak power distribution of the RRC pulses. The number of RRC pulses was 100000. The peak power is normalized using the incident peak power in the first span. As shown in Fig. 1, in each span, the peak power decreases with the increase of transmission length because the accumulated CD impairment leads to pulse

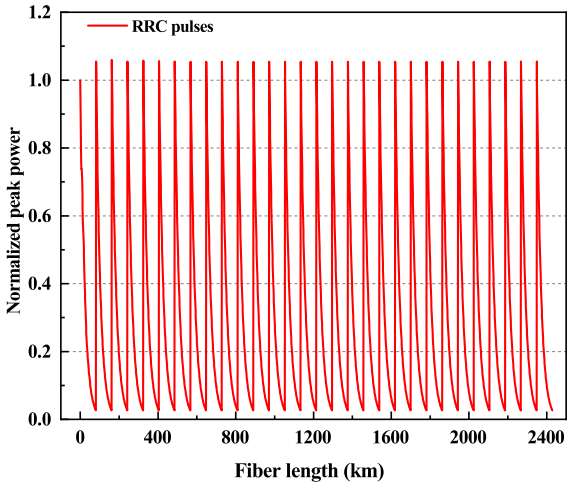


Fig. 1. The normalized peak power distribution of the RRC pulses in single-channel Nyquist 64 GBaud system.

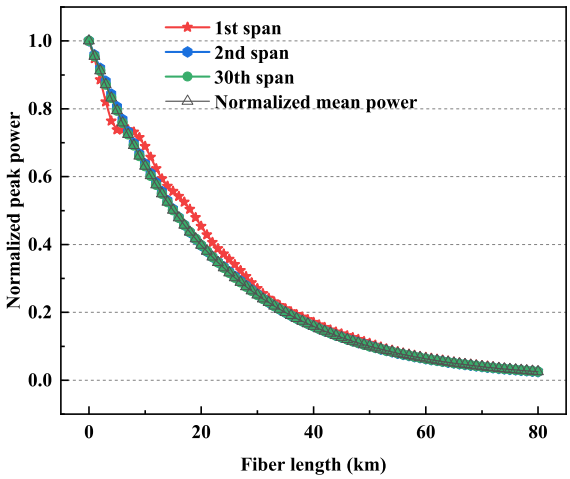


Fig. 2. The normalized peak power distribution of the RRC pulses in the 1st, 2nd, and 30th span, and the normalized mean power distribution in 64 GBaud system, respectively.

broadening. The pulse broadening weakens the peak power of the pulse, and the Kerr nonlinearity becomes weak [27].

Fig. 2 shows the normalized peak power distribution of the RRC pulses $s(t)$ in the 1st, 2nd, and 30th span and the normalized mean power distribution over 30 $\times$ 80 km SSMF in single-channel Nyquist 64 GBaud optical transmission system, respectively. In each span, peak power is normalized using the maximum peak power in the current span. As shown in Fig. 2, the peak power distribution of the RRC pulses will converge to the mean power distribution after one span of SSMF transmission. In each span, the normalized mean power only depends on the attenuation coefficient $\alpha$ and is calculated by

$$P(z) = e^{-\alpha z} \tag{7}$$

Both in the CS-DBP [14], [15], [16] and LS-DBP algorithms [17], [18], nonlinear coefficient $\gamma_{\mathrm{DBP,n}}$ is optimized based on the mean power at step position $z_n$ and expressed as

$$\gamma_{\mathrm{DBP,n}} = \gamma_{\mathrm{DBP}} e^{-\alpha z_n}, n = 1, 2, \ldots, N \tag{8}$$

where $z_n = z_{n-1} + \Delta z_n$ is the $n$th step position of the DBP algorithm. $\gamma_{\mathrm{DBP}}$ is the nonlinear coefficient which needs to be optimized. However, when the number of steps per span is fixed below the optimum step number to constrain computational complexity, the optimum nonlinear coefficient of both the CS-DBP and LS-DBP algorithms is smaller than that of the optical fiber. And the optimum nonlinear coefficient is sensitive to the number of steps per span [13]. To make the optimum nonlinear coefficient robust to the number of steps per span, we use the average value of the mean power over the step size $\Delta z_n$ instead of the mean power at the step position $z_n$. The nonlinear coefficient $\gamma_{\mathrm{DBP,n}}$ is expressed as

$$\gamma_{\mathrm{DBP,n}} = \gamma_{\mathrm{DBP}} \frac{1}{z_n - z_{n-1}} \int_{z_{n-1}}^{z_n} P(z) dz, n = 1, 2, \ldots, N \tag{9}$$

The modified mean-power-distribution-based nonlinear coefficient optimization scheme is used for CS-DBP (MMPD-CS-DBP) and LS-DBP (MMPD-LS-DBP) algorithms, respectively. Fig. 3 shows the flow chart of the MMPD-CS-DBP and MMPD-LS-DBP algorithms. The asymmetric form of the SSFM is used. $N_{\mathrm{span}}$ is the span number. Firstly, the mean power distribution $P(z)$ of the RRC pulses is simulated using SSFM. Step size $\Delta z_n$ and step position $z_n$ are calculated, respectively. Then, the nonlinear coefficient is expressed as (9). Finally, the CD and SPM are compensated step by step. Meanwhile, the value of $\gamma_{\mathrm{DBP}}$ is swept over a [0, $2\gamma$] range, performing a simulation at each value and find the optimum nonlinear coefficient $\gamma_{\mathrm{DBP,Opt}}$.

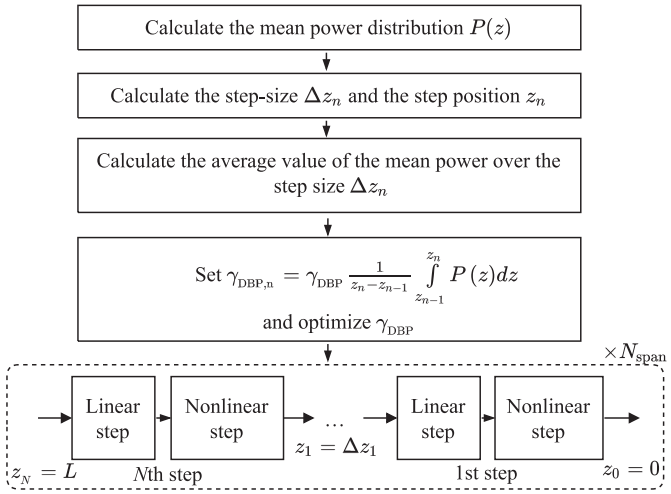


Fig. 3. The flow chart of the MMPD-CS-DBP and MMPD-LS-DBP algorithms.

## III. Simulation Results and Analysis

### A. Single-Channel Nyquist 64 GBaud PM-16QAM Optical Transmission System

Firstly, we investigated the optimum nonlinear coefficient $\gamma_{\mathrm{DBP,Opt}}$ and the nonlinearity compensation performance of

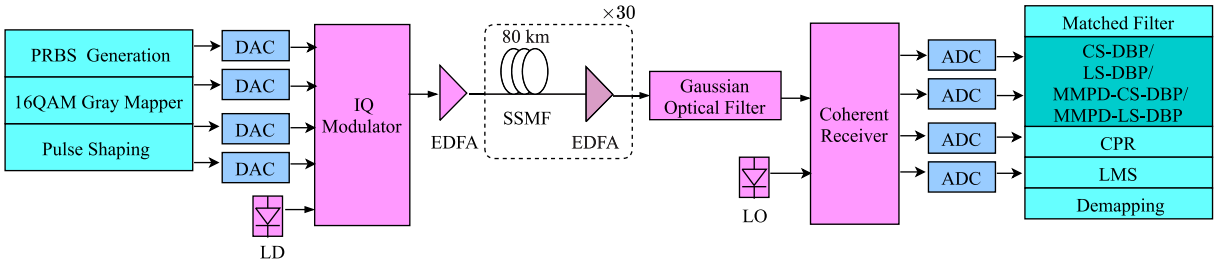


Fig. 4. The simulation single-channel Nyquist 30 × 80 km SSMF 64 GBaud PM-16QAM optical transmission system. LD: laser diode, LO: local oscillator, DAC: digital-to-analog converter, ADC: analog-to-digital converter.

TABLE I
THE PARAMETERS OF THE SIMULATION SYSTEM

| Parameters | Value |
|---|---|
| Attenuation coefficient $\alpha$ | 0.2 dB/km |
| Dispersion coefficient $\beta_2$ | $-21$ ps$^2$/km |
| Nonlinear coefficient $\gamma$ | 1.2 W$^{-1}$km$^{-1}$ |
| Polarization mode dispersion (PMD) | 0 |
| EDFA gain | 16 dB |
| EDFA Noise Figure | 4 dB |

the CS-DBP, LS-DBP, MMPD-CS-DBP, and MMPD-LS-DBP algorithms in single-channel Nyquist 64 GBaud PM-16QAM system over 30 × 80 km SSMF. The simulation system was built using commercial software VPItransmissionMakerTM 9.5, as shown in Fig. 4. Table I shows the parameters of the simulation system. At the transmitter side, the pseudo-random binary sequence (PRBS) generator was used to generate Gray-encoded dual-polarization 16QAM symbols with RRC pulse shaping. The roll-off factor was 0.005. The number of the 16QAM symbols for each polarization was 131072. To ensure accuracy in the simulation of the fiber forward propagation, the overall signal field was sampled at 16 samples per symbol. At the receiver side, matched RRC filter was used to reduce ISI. Then, the 16QAM symbols were down-sampled to 2 samples/symbol. The CS-DBP, LS-DBP, MMPD-CS-DBP, and MMPD-LS-DBP algorithms were used to compensate for CD and SPM. After the DBP algorithm, the 16QAM symbols were down-sampled to 1 sample/symbol. Then, carrier-phase recovery (CPR) and least mean square (LMS) were implemented. LMS algorithm can equalize the residual linear impairment to reduce the bit error ratio (BER) of system. Finally, the 16QAM symbols were de-modulated, and BER and Q-factor were calculated. Q-factor was calculated from BER through Q-factor $(\mathrm{dB}) = 20\lg(\sqrt{2}\mathrm{erfc}^{-1}(2\mathrm{BER}))$.

Fig. 5 shows the optimum nonlinear coefficient $\gamma_{\mathrm{DBP,Opt}}$ of the CS-DBP, LS-DBP, MMPD-CS-DBP, and MMPD-LS-DBP algorithms versus step number per span in single-channel Nyquist 64 GBaud system, respectively. The value of $\gamma_{\mathrm{DBP}}$ was optimized for each number of steps per span. As shown in Fig. 5, the $\gamma_{\mathrm{DBP,Opt}}$ of the CS-DBP and LS-DBP algorithms was sensitive to the number of steps per span. As the number of steps per span increased, the $\gamma_{\mathrm{DBP,Opt}}$ of the CS-DBP and LS-DBP

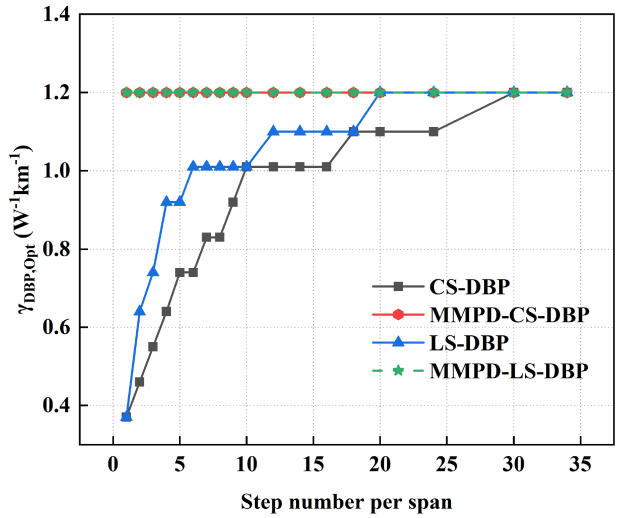


Fig. 5. The optimum nonlinear coefficient $\gamma_{\mathrm{DBP,Opt}}$ of the CS-DBP, LS-DBP, MMPD-CS-DBP, and MMPD-LS-DBP algorithms versus step number per span in single-channel Nyquist 64 GBaud system, respectively.

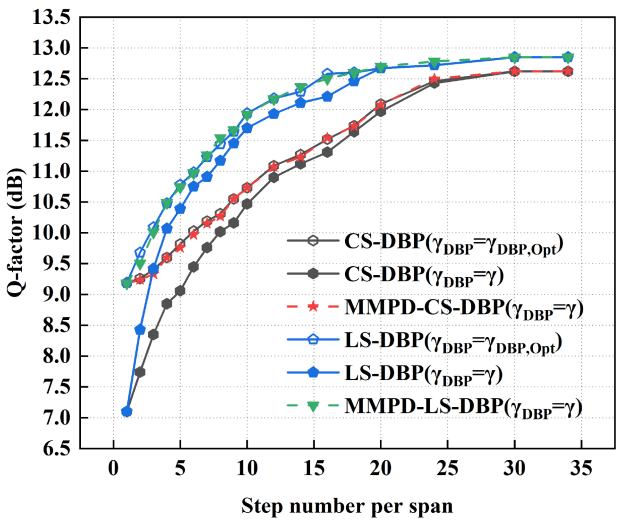


Fig. 6. The Q-factor of the CS-DBP, LS-DBP, MMPD-CS-DBP, and MMPD-LS-DBP algorithms versus the step number per span in single-channel Nyquist 64 GBaud system, respectively.

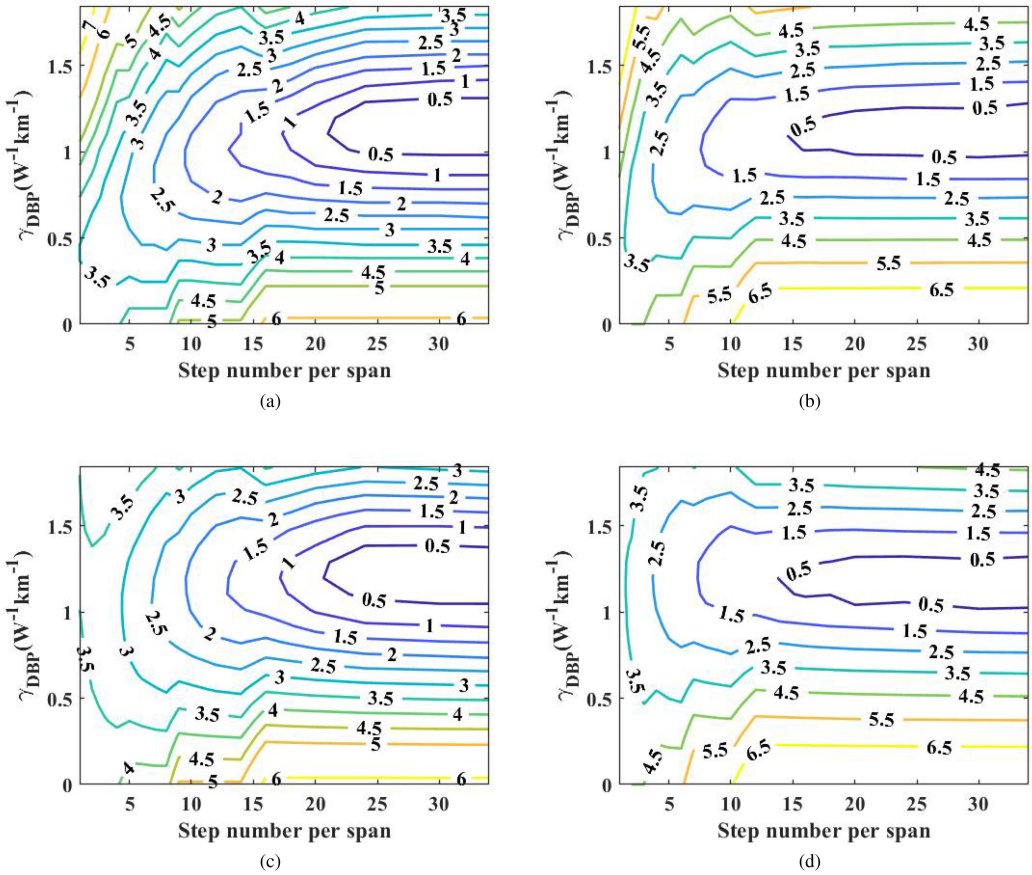


Fig. 7. Q-factor optimization in the step number per span and the nonlinear coefficient for (a) CS-DBP, (b) LS-DBP, (c) MMPD-CS-DBP, and (d) MMPD-LS-DBP algorithms in single-channel Nyquist 64 GBaud system. Labels indicated the Q-factor penalty in dB compared to the maximum value.

algorithms converged to the nonlinear coefficient of the optical fiber $\gamma = 1.2\ \mathrm{W^{-1}km^{-1}}$. The $\gamma_{\mathrm{DBP,Opt}}$ of the MMPD-CS-DBP and MMPD-LS-DBP algorithms was 1.2 $\mathrm{W^{-1}km^{-1}}$ at each number of steps per span, which meant that the $\gamma_{\mathrm{DBP,Opt}}$ of the MMPD-CS-DBP and MMPD-LS-DBP algorithms was robust to the number of steps per span.

Fig. 6 shows the Q-factor of the CS-DBP, LS-DBP, MMPD-CS-DBP, and MMPD-LS-DBP algorithms versus the step number per span in single-channel Nyquist 64 GBaud system, respectively. As shown in Fig. 6, the Q-factor performance was improved by increasing the step number per span for four DBP algorithms. As the number of steps per span increased to a certain value, the Q-factor approached the maximum value. Thus, there was an optimum step number for the DBP algorithm. The optimum step number of the CS-DBP and MMPD-CS-DBP algorithms was 30. The optimum step number of the LS-DBP and MMPD-LS-DBP algorithms was 20. At $\gamma_{\mathrm{DBP}} = \gamma = 1.2$ $\mathrm{W^{-1}km^{-1}}$, the MMPD-CS-DBP (MMPD-LS-DBP) algorithm outperformed CS-DBP (LS-DBP) algorithm when the number of steps per span was fixed below the optimum step number. The CS-DBP (LS-DBP) algorithm can achieve the same Q-factor as the MMPD-CS-DBP (MMPD-LS-DBP) algorithm by optimizing the nonlinear coefficient as $\gamma_{\mathrm{DBP}} = \gamma_{\mathrm{DBP,Opt}}$.

The Q-factor penalty versus both the step number per span and the nonlinear coefficient was calculated from the simulation results and was shown in Fig. 7. Q-factor penalty was defined as the penalty from the maximum Q-factor. As shown in Fig. 6, the maximum Q-factor of the CS-DBP and MMPD-CS-DBP

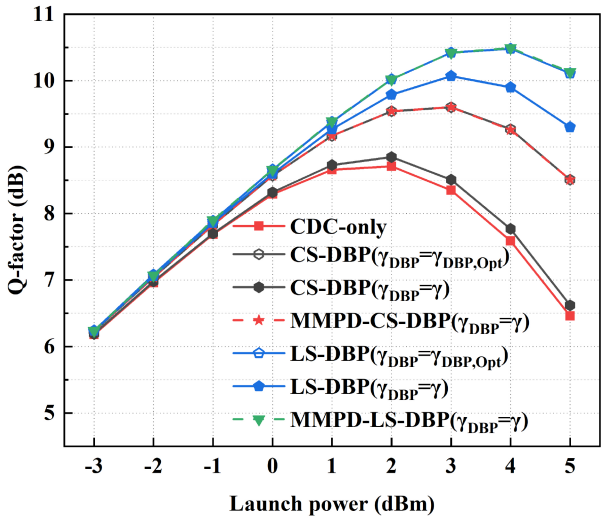


Fig. 8. The Q-factor of the CS-DBP, LS-DBP, MMPD-CS-DBP, and MMPD-LS-DBP algorithms with 4 steps/span versus launch power in single-channel Nyquist 64 GBaud system, respectively.

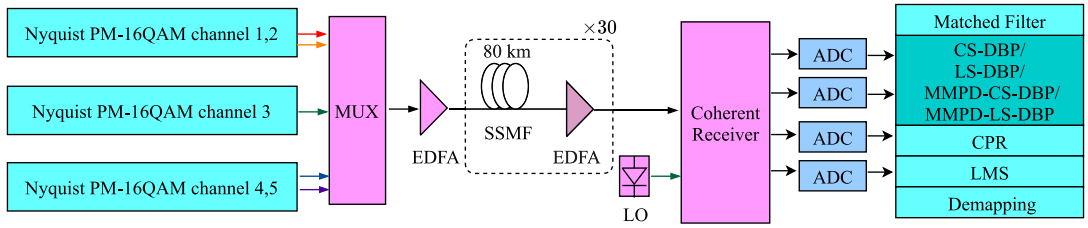


Fig. 9. The simulation 30 × 80 km SSMF 5 × 64 GBaud Nyquist WDM PM-16QAM system with 65 GHz sub-channel spacing. LD: laser diode, LO: local oscillator, DAC: digital-to-analog converter, ADC: analog-to-digital converter.

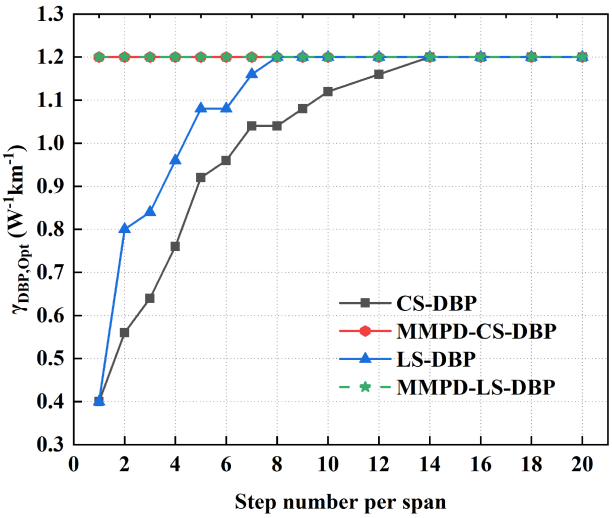


Fig. 10. The optimum nonlinear coefficient $\gamma_{\mathrm{DBP,Opt}}$ of the CS-DBP, LS-DBP, MMPD-CS-DBP, and MMPD-LS-DBP algorithms versus step number per span in 5 × 64 GBaud Nyquist WDM systems, respectively.

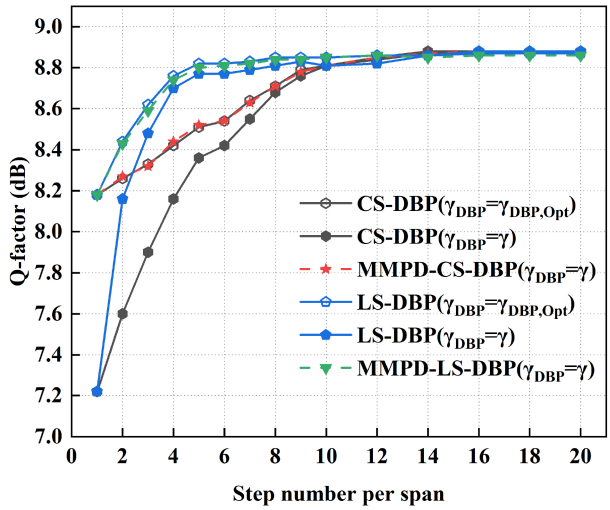


Fig. 11. The Q-factor of the center channel 3 using CS-DBP, LS-DBP, MMPD-CS-DBP, and MMPD-LS-DBP algorithms versus step number per span in 5 × 64 GBaud Nyquist WDM system, respectively.

algorithms was 12.6 dB, and the maximum Q-factor of the LS-DBP and MMPD-LS-DBP algorithms was 12.8 dB. As shown in Fig. 7(a) and (b), the lowest penalty of the CS-DBP and LS-DBP algorithms was achieved for the values of $\gamma_{\mathrm{DBP}}$ smaller than 1.2 $\mathrm{W^{-1}km^{-1}}$, in the case, that the number of steps per span was fixed below the optimal step number. As the step number was increased, $\gamma_{\mathrm{DBP,Opt}}$ converged to 1.2 $\mathrm{W^{-1}km^{-1}}$. As shown in Fig. 7(c) and (d), the lowest penalty of the MMPD-CS-DBP and MMPD-LS-DBP algorithms was achieved when the nonlinear coefficient $\gamma_{\mathrm{DBP}}$ was 1.2 $\mathrm{W^{-1}km^{-1}}$.

Fig. 8 shows the Q-factor versus launch power in single-channel Nyquist 64 GBaud system using CS-DBP, LS-DBP, MMPD-CS-DBP, and MMPD-LS-DBP algorithms with 4 steps/span, respectively. CDC-only represents CD compensation only. At $\gamma_{\mathrm{DBP}} = \gamma = 1.2$ $\mathrm{W^{-1}km^{-1}}$, CS-DBP and LS-DBP with 4 steps/span outperformed CDC-only by 0.1 dB and 1.3 dB, respectively. MMPD-CS-DBP and MMPD-LS-DBP can produce extra 0.8 dB and 0.4 dB gains over CS-DBP and LS-DBP with 4 steps/span, respectively. Moreover, the optimum launch power can be increased by 1 dB. The CS-DBP (LS-DBP) algorithm can achieve the same Q-factor as the MMPD-CS-DBP (MMPD-LS-DBP) algorithm by optimizing the nonlinear coefficient as $\gamma_{\mathrm{DBP}} = \gamma_{\mathrm{DBP,Opt}}$.

### *B. 5 × 64 GBaud Nyquist WDM PM-16QAM System With 65 GHz Sub-Channel Spacing*

We investigated the optimum nonlinear coefficient $\gamma_{\mathrm{DBP,Opt}}$ and the nonlinearity compensation performance of the CS-DBP, LS-DBP, MMPD-CS-DBP, and MMPD-LS-DBP algorithms to compensate for the nonlinear impairments in 5 × 64 GBaud Nyquist WDM PM-16QAM system with 65 GHz spacing over 30 × 80 km SSMF. Fig. 9 shows the simulation Nyquist WDM system. Table I shows the parameters of the simulation system. On the receiver side, the coherent receiver was assumed to be ideal and with no bandwidth limitation. The matched filter with 65 GHz bandwidth was used to select the central channel 3.

Fig. 10 shows the optimum nonlinear coefficient $\gamma_{\mathrm{DBP,Opt}}$ of the CS-DBP, LS-DBP, MMPD-CS-DBP, and MMPD-LS-DBP algorithms versus step number per span in 5 × 64 GBaud Nyquist WDM systems, respectively. As shown in Fig. 10, the $\gamma_{\mathrm{DBP,Opt}}$ of the CS-DBP and LS-DBP algorithms was sensitive to step number per span. As the number of steps per span increased, the $\gamma_{\mathrm{DBP,Opt}}$ of the CS-DBP and LS-DBP algorithms converged to the nonlinear coefficient of the optical fiber $\gamma = 1.2$ $\mathrm{W^{-1}km^{-1}}$. The $\gamma_{\mathrm{DBP,Opt}}$ of the MMPD-CS-DBP and MMPD-LS-DBP algorithms was $\gamma = 1.2$ $\mathrm{W^{-1}km^{-1}}$ at each number of steps per span.

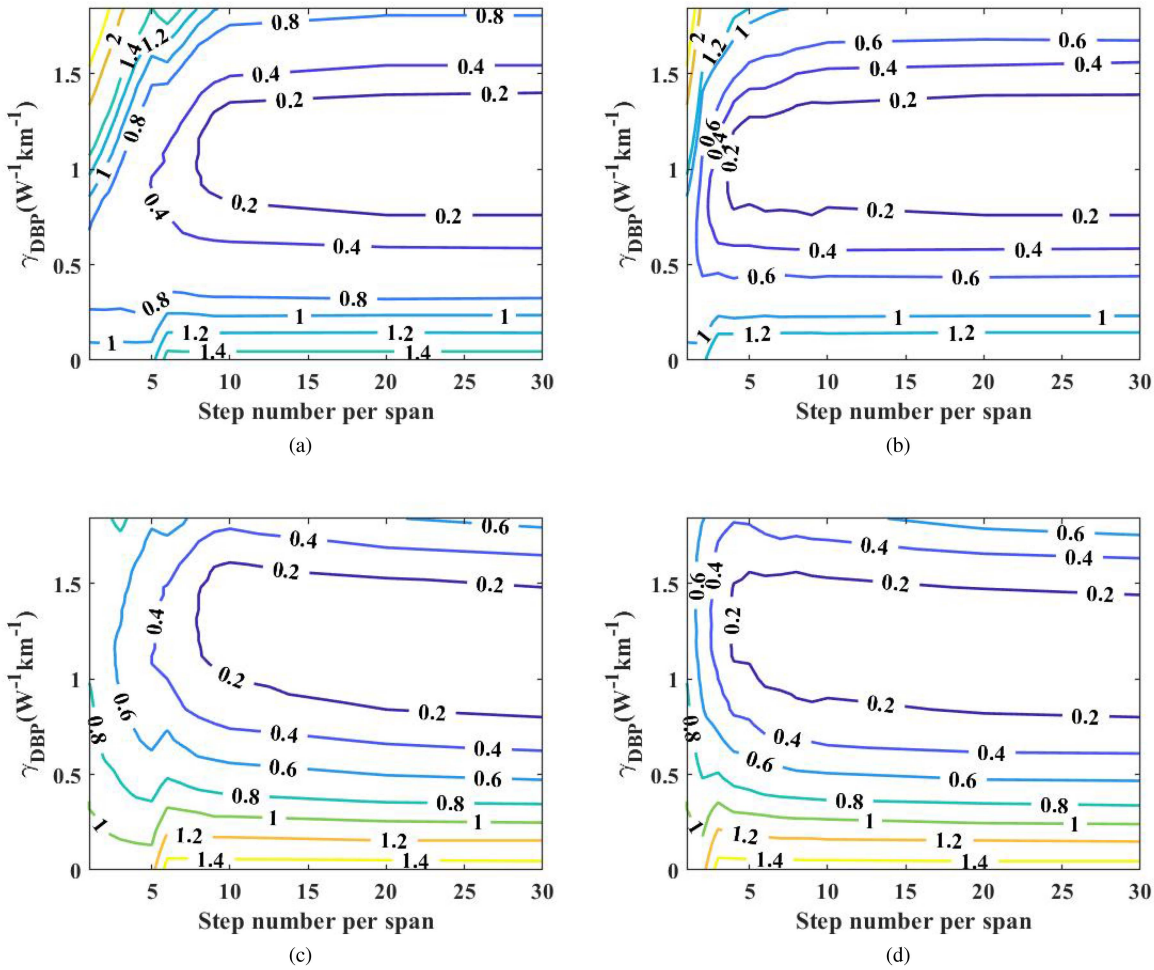


Fig. 12. The Q-factor optimization of the center channel 3 in the step number per span and the nonlinear coefficient for (a) CS-DBP, (b) LS-DBP, (c) MMPD-CS-DBP, and (d) MMPD-LS-DBP algorithms in 5 × 64 GBaud Nyquist WDM system, respectively. Labels indicated the Q-factor penalty in dB compared to the maximum value.

Fig. 11 shows the Q-factor of the center channel 3 using CS-DBP, LS-DBP, MMPD-CS-DBP, and MMPD-LS-DBP algorithms versus step number per span in 5 × 64 GBaud Nyquist WDM systems, respectively. As shown in Fig. 11, the optimum step number of the CS-DBP and MMPD-CS-DBP algorithms was 14, and the optimum step number of the LS-DBP and MMPD-LS-DBP algorithms was 8. The maximum Q-factor of the four DBP algorithms was 8.9 dB. At $\gamma_{\mathrm{DBP}} = \gamma = 1.2\ \mathrm{W}^{-1}\mathrm{km}^{-1}$, the MMPD-CS-DBP (MMPD-LS-DBP) algorithm outperformed CS-DBP (LS-DBP) algorithm when the number of steps per span was less than the optimum step number. The CS-DBP (LS-DBP) algorithm can achieve the same Q-factor as the MMPD-CS-DBP (MMPD-LS-DBP) algorithm by optimizing the nonlinear coefficient as $\gamma_{\mathrm{DBP}} = \gamma_{\mathrm{DBP,Opt}}$.

Fig. 12 shows the Q-factor penalty of the center channel 3 using CS-DBP, LS-DBP, MMPD-CS-DBP, and MMPD-LS-DBP algorithms versus both the step number per span and the nonlinear coefficient in 5 × 64 GBaud Nyquist WDM system, respectively. As shown in Fig. 12(a) and (b), when the number of steps per span was fixed below the optimum step number, the lowest penalty of the CS-DBP and LS-DBP algorithms was achieved for the values of $\gamma_{\mathrm{DBP}}$ smaller than 1.2 $\mathrm{W}^{-1}\mathrm{km}^{-1}$. As the step size was decreased, $\gamma_{\mathrm{DBP,Opt}}$ converged to 1.2 $\mathrm{W}^{-1}\mathrm{km}^{-1}$. As shown in Fig. 12(c) and (d), the lowest penalty of the MMPD-CS-DBP and MMPD-LS-DBP algorithms was achieved when the values of $\gamma_{\mathrm{DBP}}$ was 1.2 $\mathrm{W}^{-1}\mathrm{km}^{-1}$.

Fig. 13 shows the Q-factor of the center channel 3 using CS-DBP, LS-DBP, MMPD-CS-DBP, and MMPD-LS-DBP algorithms with 2 steps/span versus launch power in 5 × 64 GBaud Nyquist WDM system, respectively. As Fig. 13 shows, compared with the optimum Q-factor of the CDC-only in single-channel Nyquist 64 GBaud system, the optimum Q-factor of the CDC-only was reduced from 8.7 dB to 7.8 dB due to the Kerr nonlinearity of XPM and FWM. At $\gamma_{\mathrm{DBP}} = \gamma = 1.2\,\mathrm{W}^{-1}\mathrm{km}^{-1}$, LS-DBP algorithm outperformed CDC-only by 0.4 dB. However, CS-DBP algorithm can not effectively compensate for the nonlinear impairments. MMPD-CS-DBP and MMPD-LS-DBP algorithms can produce extra 0.5 dB and 0.2 dB gains over CS-DBP and LS-DBP, respectively. The CS-DBP (LS-DBP) algorithm can achieve the same Q-factor as the MMPD-CS-DBP (MMPD-LS-DBP) algorithm by optimizing the nonlinear coefficient as $\gamma_{\mathrm{DBP}} = \gamma_{\mathrm{DBP,Opt}}$.

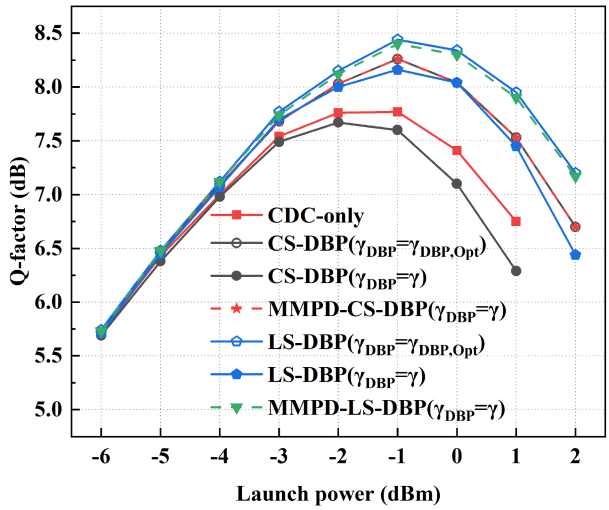


Fig. 13. The Q-factor of the center channel 3 using CS-DBP, LS-DBP, MMPD-CS-DBP, and MMPD-LS-DBP algorithms with 2 steps/span versus launch power in 5 × 64 GBaud Nyquist WDM system, respectively.

## IV. Conclusion

In this paper, we proposed a modified mean-power-distribution-based nonlinear coefficient optimization scheme for the DBP algorithm. In the proposed scheme, the nonlinear coefficient was optimized based on the average value of the mean power over the step size. The proposed scheme was applied with CS-DBP and LS-DBP algorithms to investigate the optimum nonlinear coefficient and nonlinearity compensation performance in the simulation transmissions of single-channel Nyquist 64 GBaud and 5 × 64 GBaud Nyquist WDM PM-16QAM symbols over 30 × 80 km SSMF, respectively. Simulation results showed that the optimum nonlinear coefficient of the MMPD-CS-DBP and MMPD-LS-DBP algorithms is the nonlinear coefficient of the optical fiber and is robust to the number of steps per span. Therefore, the modified mean-power-distribution-based nonlinear coefficient optimization scheme can effectively simplify the nonlinear coefficient optimization of the DBP algorithm.

## References

[1] P. J. Winzer, "High-spectral-efficiency optical modulation formats," *J. Lightw. Technol.*, vol. 30, no. 24, pp. 3824–3835, Dec. 2012.
[2] S. Chandrasekhar and X. Liu, "OFDM based superchannel transmission technology," *J. Lightw. Technol.*, vol. 30, no. 24, pp. 3816–3823, Dec. 2012.
[3] U. Cisco, "Cisco annual internet report(2018–2023) white paper. 2020," *Acessado em*, vol. 10, no. 01, pp. 1–35, 2021.
[4] F. Buchali, K. Schuh, L. Schmalen, W. Idler, E. Lach, and A. Leven, "1-Tbit/s dual-carrier DP 64QAM transmission at 64Gbaud with 40% overhead soft-FEC over 320 km SSMF," in *Proc. Opt. Fiber Commun. Conf.*, Optical Society of America, 2013, pp. 1–3.
[5] W. Idler, F. Buchali, and K. Schuh, "Experimental study of symbol-rates and MQAM formats for single carrier 400 Gb/s and few carrier 1 Tb/s options," in *Proc. Opt. Fiber Commun. Conf. Exhib.*, 2016, pp. 1–3.
[6] K. Schuh et al., "Single carrier 1.2 Tbit/s transmission over 300 km with PM-64 QAM at 100 GBaud," in *Proc. Opt. Fiber Commun. Conf.*, 2017, pp. 1–3.
[7] J. H. Ke, Y. Gao, and J. C. Cartledge, "400 Gbit/s single-carrier and 1 Tbit/s three-carrier superchannel signals using dual polarization 16-QAM with look-up table correction and optical pulse shaping," *Opt. Exp.*, vol. 22, no. 1, pp. 71–83, 2014.
[8] R. Rios-Müller et al., "Spectrally-efficient 400-Gb/s single carrier transport over 7200 km," *J. Lightw. Technol.*, vol. 33, no. 7, pp. 1402–1407, Apr. 2015.
[9] G. Raybon et al., "Single-carrier 400 G interface and 10-channel WDM transmission over 4,800 km using all-ETDM 107-Gbaud PDM-QPSK," in *Proc. Opt. Fiber Commun. Conf. Expo. Nat. Fiber Optic Engineers Conf.*, 2013, pp. 1–4.
[10] D. Semrau, D. Lavery, L. Galdino, R. I. Killey, and P. Bayvel, "The impact of transceiver noise on digital nonlinearity compensation," *J. Lightw. Technol.*, vol. 36, no. 3, pp. 695–702, Feb. 2018.
[11] A. Ellis, M. McCarthy, M. Al Khateeb, M. Sorokina, and N. Doran, "Performance limits in optical communications due to fiber nonlinearity," *Adv. Opt. Photon.*, vol. 9, no. 3, pp. 429–503, 2017.
[12] X. Liu, A. R. Chraplyvy, P. J. Winzer, R. W. Tkach, and S. Chandrasekhar, "Phase-conjugated twin waves for communication beyond the Kerr nonlinearity limit," *Nature Photon.*, vol. 7, no. 7, pp. 560–568, 2013.
[13] G. Liga, T. Xu, A. Alvarado, R. I. Killey, and P. Bayvel, "On the performance of multichannel digital backpropagation in high-capacity long-haul optical transmission," *Opt. Exp.*, vol. 22, no. 24, pp. 30053–30062, 2014.
[14] E. Ip and J. M. Kahn, "Compensation of dispersion and nonlinear impairments using digital backpropagation," *J. Lightw. Technol.*, vol. 26, no. 20, pp. 3416–3425, Oct. 2008.
[15] E. Ip, "Nonlinear compensation using backpropagation for polarization-multiplexed transmission," *J. Lightw. Technol.*, vol. 28, no. 6, pp. 939–951, Mar. 2010.
[16] E. Temprana, E. Myslivets, L. Liu, V. Ataie, and S. Radic, "Two-fold transmission reach enhancement enabled by transmitter-side digital backpropagation and optical frequency comb-derived information carriers," *Opt. Exp.*, vol. 23, no. 16, pp. 20774–20783, 2015.
[17] R. Asif, C. Y. Lin, M. Holtmannspoetter, and B. Schmauss, "Logarithmic step-size based digital backward propagation in N-channel 112Gbit/s/ch DP-QPSK transmission," in *Proc. 13th Int. Conf. Transp. Opt. Netw.*, 2011, pp. 1–4.
[18] J. Zhang, X. Li, and Z. Dong, "Digital nonlinear compensation based on the modified logarithmic step size," *J. Lightw. Technol.*, vol. 31, no. 22, pp. 3546–3555, Nov. 2013.
[19] D. Rafique, M. Mussolin, M. Forzati, J. Mårtensson, M. N. Chugtai, and A. D. Ellis, "Compensation of intra-channel nonlinear fiber impairments using simplified digital back-propagation algorithm," *Opt. Exp.*, vol. 19, no. 10, pp. 9453–9460, 2011.
[20] M. Secondini, D. Marsella, and E. Forestieri, "Enhanced split-step Fourier method for digital backpropagation," in *Proc. Eur. Conf. Opt. Commun.*, 2014, pp. 1–3.
[21] P. He, A. Yang, P. Guo, Y. Qiao, and X. Xin, "A layer-reduced neural network based digital backpropagation algorithm for fiber nonlinearity mitigation," *IEEE Photon. J.*, vol. 13, no. 3, pp. 1–12, Jun. 2021.
[22] M. Yang, P. He, A. Yang, and P. Guo, "Peak power distribution based nonlinear parameter optimization for digital back-propagation," in *Proc. Asia Commun. Photon. Conf.*, 2021, pp. 1–3.
[23] H. N. Tan and S. T. Le, "On the effectiveness of nonlinearity compensation for high-baudrate single-channel transmissions," *Opt. Commun.*, vol. 433, pp. 36–43, 2019.
[24] N. V. Dien et al., "Digital back-propagation optimization for high-baudrate single-channel optical fiber transmissions," *Opt. Commun.*, vol. 491, 2021, Art. no. 126913.
[25] C. Häger and H. D. Pfister, "Wideband time-domain digital backpropagation via subband processing and deep learning," in *Proc. Eur. Conf. Opt. Commun.*, 2018, pp. 1–3.
[26] J. Wang, C. Xie, and Z. Pan, "Generation of spectrally efficient Nyquist-WDM QPSK signals using digital FIR or FDE filters at transmitters," *J. Lightw. Technol.*, vol. 30, no. 23, pp. 3679–3686, Dec. 2012.
[27] G. P. Agrawal, *Fiber-Optic Communication Systems*. Hoboken, NJ, USA: Wiley, 2012.